

Cluster Spin Glass Distribution Functions in $\text{La}_{2-x}\text{Sr}_x\text{CuO}_4$ *

R.S. Markiewicz⁽¹⁾, F. Cordero⁽²⁾, A. Paolone⁽³⁾, and R. Cantelli⁽³⁾

(1) *Physics Department and Barnett Institute,
Northeastern U., Boston MA 02115;*

(2) *CNR Roma, Istituto di Acustica "O.M. Corbino", Roma, Italy;*

(3) *Dept. of Physics, University of Roma "La Sapienza" and Unità INFN di Roma, Italy*

Signatures of the cluster spin glass have been found in a variety of experiments, with an effective onset temperature T_{on} that is frequency dependent. We reanalyze the experimental results and find that they are characterized by a distribution of activation energies, with a nonzero glass transition temperature $T_g(x) < T_{on}$. While the distribution of activation energies is the same, the distribution of weights depends on the process. Remarkably, the weights are essentially doping independent.

I. INTRODUCTION

Hole doping in the cuprates is now widely believed to lead to strongly inhomogeneous phases, with the holes being ejected from the antiferromagnetic domains onto antiphase boundaries. Ordering of these charged stripe walls leads to a form of domain phase, which is typically dynamic. In the very low doping limit, the inhomogeneity is manifested in the form of transverse spin freezing in the antiferromagnetic phase,¹ and, when the Néel temperature $T_N \rightarrow 0$, as a ‘cluster spin glass’ (CSG).² Wakimoto, et al. (WUEY)³ have correlated a number of experimental observations of this CSG in $\text{La}_{2-x}\text{Sr}_x\text{CuO}_4$ (LSCO), and raise the issue of whether there is a real finite temperature glass transition, or just a continuous relaxational slowing down. On the one hand, all of the experiments find the transition at a different temperature, depending on the time scale of the measurement; on the other hand, the susceptibility shows striking scaling behavior, both with temperature and applied field.

Here, we analyze these data in more detail, combining them with additional measurements at intermediate frequencies. In all measurements, we find that the CSG freezing turns on at an onset temperature T_{on} which scales with the logarithm of the measurement frequency, consistent with a relaxational form,

$$I \simeq \frac{\omega\tau}{1 + \omega^2\tau^2} \quad (1)$$

with Vogel-Fulcher⁴ relaxation

$$\tau = \tau_0 e^{E/(T-T_g)} \quad (2)$$

(here T_{on} corresponds to the temperature below which τ^{-1} becomes slower than the measuring angular frequency ω). In order to explain the observed scaling behavior, we find that the CSG must have a broad distribution of activation energies, with a well defined characteristic energy scale E_m , and that different experiments probe different aspects of this distribution.

II. T_G AND ACTIVATION ENERGY DISTRIBUTION FUNCTIONS

The glass transition temperature T_g is typically found by looking for deviations from activated behavior: curvature in a plot of $\ln(\omega)$ vs. $1/T$ (here, ω is a characteristic frequency of a given experiment and T is the temperature). The presence of a broad distribution of activation energies makes it difficult to extract a unique value of T_g . For the CSG, there is an additional complicating factor: the characteristic frequencies are often not well defined. For instance, in the neutron diffraction experiments,⁵ the effective frequency is taken as the energy resolution 0.25meV: the diffraction peak is elastic, or static, on that energy scale. On the other hand, the magnetic susceptibility was measured by a ‘static’ SQUID technique;³ since a typical scan takes about 10 s,⁶ we assume an effective frequency of $\sim 1/20$ Hz. Clearly, improved determination of these frequencies will lead to better estimates for T_g – particularly at the lowest frequencies. Nevertheless, the variation with frequency is so striking that the qualitative features should be unchanged by these refinements.

The simplest distribution comes from measuring the magnetic susceptibility $\chi_0(T)$. WUEY found that the in-plane χ_0 could be fit to a simple Curie law with small Curie constant for temperatures between 10 K and 70 K, while at lower temperatures the Curie constant became temperature dependent as clusters began to freeze out. To analyze these results, we assume that the susceptibility has a relaxational component

$$\chi_0(T) \equiv \chi_C(T)(1 - q) = \int dE w_{sus}(E) \frac{\chi_C}{1 + \omega^2\tau(E)^2}, \quad (3)$$

with χ_C the Curie susceptibility and $w_{sus}(E)$ the susceptibility distribution function. This distribution function has a simple interpretation in the standard model of

*This work has been carried out in the framework of the Progetto di Ricerca Avanzato INFN-SPIS.

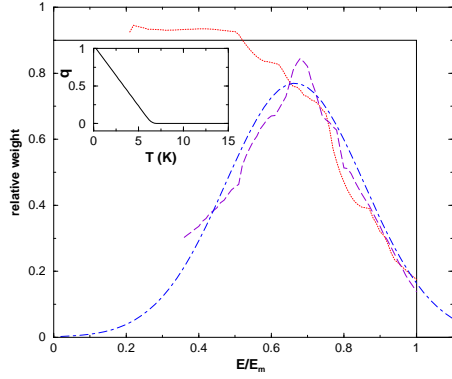


FIG. 1. Distributions of excitation energies w_{susc} (solid line), $w_{anelast}$ (dotted line), and w_{NQR} (dashed line); dot-dashed line = Gaussian approximation to w_{NQR} . Insert: resulting $q(T)$, Eq.3.

the susceptibility. It is assumed⁷ that there is a distribution of clusters, with their spins locked in an antiferromagnetic pattern, so that each cluster with an even (odd) number of spins has net spin zero (1/2). The observed Curie law is attributed to the response of the odd-spin clusters, thereby naturally explaining the small Curie constant. Since the Curie law is obeyed between 10-70 K, the clusters must have a well defined size distribution, which begins to freeze out at lower temperatures; $w_{susc}(E)$ is then the distribution of the number of clusters with a given activation energy, independent of the cluster size. If this distribution is normalized ($\int dE w_{susc}(E) = 1$), then

$$q = \int dE w_{susc}(E) \frac{\omega^2 \tau(E)^2}{1 + \omega^2 \tau(E)^2}. \quad (4)$$

The strong temperature dependence of τ , Eq.2, means that Eq. 4 can be simplified. For each temperature, there is a corresponding activation energy for which $\omega\tau(E(T)) = 1$, namely $E(T) = -T \ln(\omega\tau_0)$. Then the effective Edwards-Anderson⁸ order parameter q may be approximated

$$q \simeq \int_{E(T)}^{E_m} dE w_{susc}(E). \quad (5)$$

The observed³ scaling $q \sim (T_{on} - T)^\beta$ with $\beta \sim 1$ then suggests that $w_{susc}(E) = \text{const}$ for $E \leq E_m$, with $E_m = E(T_{on})$. Thus the appearance of T_{on} is interpreted as the presence of a sharp cutoff E_m ,

$$T_{on} = -E_m / \ln(\omega\tau_0). \quad (6)$$

The (flat) distribution of w_{susc} is shown in Figure 1; the insert to the figure shows that the above analysis is well satisfied by direct numerical integration of Eq. 3. We note that Eq. 3 has been applied⁹ for describing susceptibility data in the spin glass state ($T < T_g$); however, the above analysis depends only on the form of the distribution, and holds even if $T_g = 0$.

The above analysis can be extended to other experimental measurements. There are two changes. First, the susceptibility is proportional to the product of a coupling and a distribution function, $\chi_C(T) w_{susc}(E)$; for other properties, this can be written $A_i(T) w_i(E)$, where A_i represents the intrinsic temperature dependence of the process. In these calculations, we assume that $A_{anelast} \sim 1/T$ (Ref. 10) while $A_{NQR} \sim \text{const}$. Secondly, since most of the other probes are sampling a dissipation, there is an extra factor of $\omega\tau$ in the integrand, as in Eq.1. This factor means that the integrand at any T will be strongly peaked at $E(T)$.

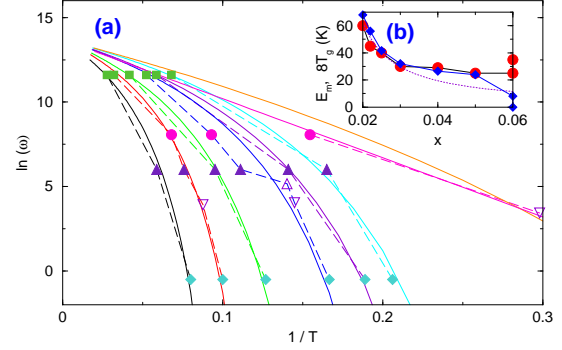


FIG. 2. (a) Scaling of effective transition temperature (corresponding to largest activation energy) with frequency. The symbols represent the measurement techniques: squares = neutron diffraction; circles = NQR; filled triangles = μ SR; open, inverted triangles = anelastic relaxation (1st mode – open triangle = 5th mode); and diamonds = susceptibility. The different sets connected by dashed lines refer to individual doping densities, from left to right: $x = 0.02, 0.022, 0.025, 0.03, 0.04, 0.05$, and 0.06 . Solid lines = fits. Insert (b): corresponding T_g (diamonds) and $E_m(x)/8$ (circles), with dotted line = fit. T_g is multiplied by 8 for comparison with E_m .

Figure 2a summarizes the doping dependence of T_{on} vs. measurement frequency. The data are, from highest frequency: squares = neutron scattering determination of the onset of (diagonal) stripe order⁵ ($\omega = 0.25$ meV = 4×10^{11} s⁻¹); circles = NQR measurements¹¹ ($\omega/2\pi = 19$ MHz); filled triangles = μ SR¹² ($\omega = 10^6$ s⁻¹); open triangles = anelastic relaxation¹¹ ($\omega/2\pi \simeq 2$ kHz); and diamonds = susceptibility³ ($\omega/2\pi \simeq 1/20$ Hz). Solid lines are fits assuming a finite glass transition temperature T_g ; Figure 2b shows the parameters $T_g(E_m)$ assumed in the fits. [In order to plot Fig. 2, it was sometimes necessary to use the smoothed curves of Ref. 3 rather than the actual data; this would only be a problem in the doping range $x \leq 0.025$, where some curves are extrapolated. Also, two fits are shown for the $x = 0.06$ data: the straight line corresponding to the larger E_m and smaller T_g ($= 0$).] While there is considerable scatter in the data, it appears that τ_0 is essentially doping independent, while E_m decreases with doping, Fig. 2b. For most dopings, the approximate relation $E_m = 8k_B T_g$ is satisfied. The

value of $\tau_0^{-1} = 5 \times 10^{13} \text{ s}^{-1} = 33 \text{ meV}$ is close to the value 22 meV estimated by Julien *et al.*¹³ from the peak in the NQR T_1^{-1} . The dotted line in Fig. 2b is a fit to the form $E_m = E_0/(x - x_0)$, with $E_0 = 0.564 \text{ K}$, $x_0 = 0.011$. The general trend $E_m \sim 1/x$ has been noted earlier.¹⁴

We have included in Fig. 2 some anelastic and NQR data for a sample with $x \sim 0.02$. Uncertainty in the precise doping makes it unclear whether the actual doping is $x \simeq 0.017$, with spin freezing transition $T_f \sim 13.9 \text{ K}$ or $x \gtrsim 0.02$, with $T_{on} \sim 10 \text{ K}$. We find that the assumption of an effective density $x_{eff} = 0.021$ yields remarkable agreement for both $T_{on}(\omega)$, but also for the weight distributions for both anelastic relaxation and NQR¹⁵, as illustrated in Figs. 4 and 5 below. Indeed, results by Curro, et al.¹⁶ show that La NMR weight distributions are very similar in the spin freezing and CSG regimes.

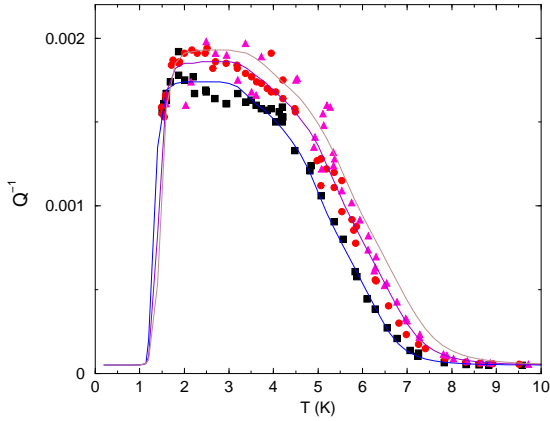


FIG. 3. Elastic energy loss coefficient, $Q^{-1}(T)$, for a $x = 0.03$ sample, by exciting the lowest three (odd) flexural modes: squares = 1st ($\omega/2\pi = 1.7 \text{ kHz}$), circles = 3rd (9.3 kHz), triangles = 5th (23 kHz). Solid lines = fit to the first mode, with distribution $w_{anelast}$ shown in Fig. 1, scaled by ω for the higher modes.

Figure 3 illustrates the fit of the elastic energy loss coefficient Q^{-1} for the three lowest odd modes of an LSCO sample at $x = 0.03$, while the corresponding distribution function is shown in Figure 1. Approximately the same distribution works for the $x \sim 0.02$ and the $x = 0.06$ samples (Fig. 4). Figure 5 shows the corresponding fits for the NQR relaxation rate; the distribution function (shown scaled in Fig. 1) was fit for the $x \sim 0.02$ sample, then scaled for the others. Note that for the anelastic response the fit is worse for the higher harmonics, and for $x \sim 0.02$ anelastic data there is an additional, lower-temperature process with a very different doping dependence.¹⁷ Also there appears to be a weak extra feature in the NQR (~ 0.02) data near 20 K. It should be cautioned that the inversion of the data to obtain the distributions, Fig. 1, is not unique: the lorentzians are sufficiently broad that several distributions could lead to

the same final spectra. The distributions chosen in Fig. 1 were chosen to be relatively smooth. [Note that the low-energy cutoffs are exaggerated, since data at sufficiently low temperatures are lacking.]

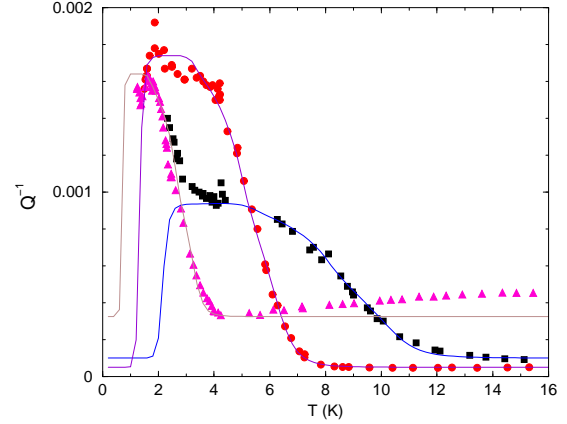


FIG. 4. Fit to the elastic energy loss coefficient, $Q^{-1}(T)$, for samples of several dopings, $x \sim 0.02$ (squares), 0.03 (circles), and 0.06 (triangles).¹⁵ All fits use the same distribution of $w_{anelast}$.

All three distributions in Fig. 1 appear to be universal, in that the same distribution holds over a wide doping range. However, different properties appear to be characterized by different distribution functions. We suggest that the different experiments may sample different attributes of the clusters. Thus, as discussed above, the susceptibility is proportional to the *number* of clusters with a particular activation energy. Since anelastic relaxation responds to the change in elastic energy when one type of domain grows at the expense of another domain with less favorable orientation, $w_{anelast}$ should be sensitive to the domain walls, namely the *perimeters* of the domains; similarly $w_{NQR}(E)$ should measure the total number of spins, or the total *areas* of all the domains with a given activation energy E .

The nearly constant Q^{-1} at low T implies a nearly constant distribution $w_{anelast}$ at low E , Fig. 1; this can be understood as follows: since

$$\begin{aligned} Q^{-1} &= \int dE \frac{w_{anelast}(E)}{T} \frac{\omega\tau}{1 + \omega^2\tau(E)^2} \\ &\simeq \int dE \frac{w_{anelast}(E)}{T} \delta(\omega\tau - 1) \\ &= \frac{w_{anelast}(E(T))}{T \left| \frac{\partial \omega\tau}{\partial E} \right|_{\omega\tau=1}} = w_{anelast}(E(T)), \end{aligned} \quad (7)$$

so when Q^{-1} is roughly constant, so is $w_{anelast}(E(T))$.

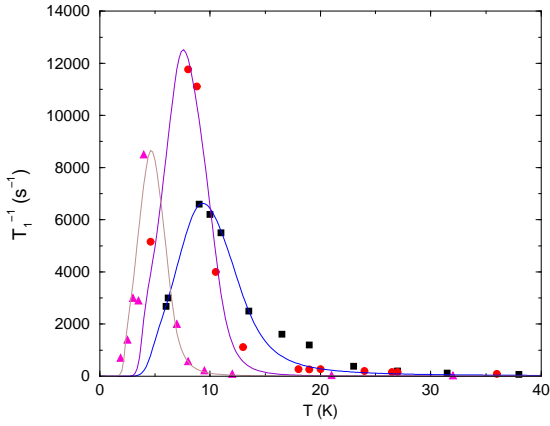


FIG. 5. Fit to NQR data T_1^{-1} for several dopings, $x \sim 0.02$ (squares), 0.03 (circles), and 0.06 (triangles). The data are from Refs. 11 and 13. All fits use the same distribution of w_{NQR} .

III. DISCUSSION

The distributions, Fig. 1, and the spin glass transition temperatures T_g are the principle results of this work. As discussed above, w_{susc} measures the cluster number distribution, $w_{anelast}$ the perimeter distribution, and w_{NQR} the area distribution. Figure 1 suggests that the perimeters and areas follow the same distribution at high energies, but that the area distribution starts to fall off sooner.

An important finding is the *universality* of the distributions: the same distributions appear to hold over a wide doping range. Earlier La NMR measurements found a similar broad distribution (fit to a Gaussian)¹⁸, and found a universal weight distribution over an even wider doping range, including spin-freezing, near-optimal superconducting, and Li-doped samples.¹⁶ Indeed, the present NQR distribution can be fit to a Gaussian, dashed line in Fig. 1,

$$w = \frac{w_0}{\sqrt{2\pi}z_A} e^{-\frac{(z-z_B)^2}{2z_A^2}}, \quad (8)$$

with $z = E/E_m$, $w_0 = 0.367$, $z_A = 0.190$, and $z_B = 0.665$.

It is possible to use the distribution functions to understand how the spin slowing down evolves with temperature, since (at any given frequency) the processes with the highest values of $E(T)$ will freeze out first. Thus the distribution $w(E)$ can be alternatively considered as a distribution $w(T)$ of the number of processes freezing out at temperature T , with $T \sim E/k_B$. From the neutron scattering, at $T_{on}(\omega)$ diagonal stripes start to order, with growing coherence length, but the coherence length cuts off at a fairly small value without diverging. At the same time the number of free clusters is decreasing (from w_{susc}). There is a large change in the number of clusters

(w_{susc}), but only a small decrease in the total number of fluctuating spins ($w_{area} = w_{NQR}$), so presumably the smallest, most strongly pinned clusters (largest $E(T)$) are freezing out. This interpretation that the clusters are small is strengthened by the fact that they make approximately the same contribution to $w_{perim} = w_{anelast}$ and $w_{area} = w_{NQR}$ (i.e., all spins are on the surface of the cluster). The fact that w_{area} is finite suggests that the spins are freezing out rather than clustering. At some point (perhaps when the correlation length stops increasing) the contribution to w_{area} drops sharply, but the cluster walls can still move. Note that even though w_{area} is shrinking, there are still many freely moving clusters (w_{susc} remains constant), suggesting that something like a ‘percolating backbone’ has frozen out, and at lower temperatures the backbone grows by capturing additional clusters.

The observed curvature in the plot of $\ln(\omega)$ vs. $1/T$ strongly suggests the existence of a well-defined finite temperature CSG transition at fixed T_g . Additional measurements, especially with well-defined low frequencies, would help pin down the value of $T_g(x)$, but should not change the overall picture. The interpretation is complicated by the presence of a broad distribution of activation energies, which lead to slowing down over a wide frequency range. In particular, we have shown that an apparent scaling of the order parameter q can arise from a particular form of $w(E)$, with sharp upper cutoff E_m . However, scaling behavior is also found in an applied magnetic field,³ and this is harder to explain. The doping dependence of E_m (insert, Fig. 2) is very suggestive of pinning effects. Note that E_m appears to diverge as $x \rightarrow x_0 \sim 0.01$, but this is cut off by the Néel transition near $x = 0.02$. We suggest that the observed behavior is characteristic of stripe freezing in the presence of defect pinning. In the absence of pinning, there could be a long range stripe ordering phase transition, but only at $T \rightarrow 0$ due to fluctuations of the walls in two dimensions. In this case, the correlation length would diverge as $T \rightarrow 0$. Impurities will tend to pin the charge stripes, but the pinning will vary in space, depending on the distribution of the impurities, and hence leading to a wide distribution of activation energies. Certainly, the large attempt frequency $\tau_0 \sim 2 \times 10^{-14}$ s (Fig. 2) is suggestive of an electronic process, $\hbar\tau_0^{-1} \sim J/4$, with J the exchange constant.

In attempting to refine the experimental determination of $T_g(x)$, it must be noted that T_{on} may be a strong function of the sensitivity of the probe to fluctuations. For instance, whereas the La NQR shows a T_{on} in the range of ~ 10 -20 K, Cu NMR is wiped out at a much higher temperature, ~ 50 K. It has been suggested^{16,13} that this wipeout is caused by the same CSG fluctuations, which are in the CuO_2 plane, and hence have a much greater effect on Cu than on La (for an alternative interpretation, see Ref. 19). A remaining puzzle is that the wipeout should start to recover below T_g ,²⁰ whereas no recovery is found for the Cu signal down to 350 mK.²¹

IV. CONCLUSION

The signatures of spin freezing in $\text{La}_{2-x}\text{Sr}_x\text{CuO}_4$ from neutron spectroscopy, NQR relaxation, anelastic relaxation and magnetic susceptibility (spanning ~ 13 orders of magnitude of frequency) have been reconsidered in terms of a distribution $w(E)$ of activation energies for the spin dynamics. Each experiment probes a different aspect of the spin clusters, like the total number of spins in a cluster, the spins along its perimeter or the number of clusters with an unpaired spin, and therefore requires a different weight function for the distribution of activation energies. It is found, however, that for each process the same $w(E/E_m(x))$ can explain all the data, independent of doping, with the same $E_m(x)$ for all the experiments. In addition, $E_m(x)$ scales linearly with the temperature $T_g(x)$ at which the effective spin fluctuation rate deduced from all the experiments freezes toward the cluster-spin glass state.

Acknowledgments: The authors thank Prof. A. Rigamonti for useful advice. One of the authors (R.S. Markiewicz) wishes to thank the University of Rome “La Sapienza” for its hospitality.

-
- ¹ F.C. Chou, F. Borsa, J.H. Cho, D.C. Johnston, A. Lascialfari, D.R. Torgeson, and J. Ziolo, Phys. Rev. Lett. **71**, 2323 (1993).
 - ² J.H. Cho, F. Borsa, D.C. Johnston, and D.R. Torgeson, Phys. Rev. B **46**, 3179 (1992).
 - ³ S. Wakimoto, S. Ueki, Y. Endoh, and K. Yamada, Phys. Rev. B **62**, 3547 (2000).
 - ⁴ H. Vogel, Phys. Z. **22**, 645 (1921); G.S. Fulcher, J. Am. Chem. Soc. **8**, 339 (1925).
 - ⁵ S. Wakimoto, G. Shirane, Y. Endoh, K. Hirota, S. Ueki, K. Yamada, R.J. Birgeneau, M.A. Kastner, Y.S. Lee, P.M. Gehring, and S.H. Lee, Phys. Rev. B **60**, 769 (1999).
 - ⁶ S. Wakimoto, personal communication.
 - ⁷ R.J. Gooding, N.M. Salem, R.J. Birgeneau, and F.C. Chou, Phys. Rev. B **55**, 6360 (1997).
 - ⁸ S.F. Edwards and P.W. Anderson, J. Phys. F **5**, 965 (1975).
 - ⁹ K.H. Fischer and J.A. Hertz, “Spin Glasses” (Cambridge, Cambridge University Press, 1991).
 - ¹⁰ A.S. Nowick and B.S. Berry *Anelastic Relaxation in Crystalline Solids* (Academic, 1973).
 - ¹¹ A. Campana, M. Corti, A. Rigamonti, R. Cantelli, and F. Cordero, cond-mat/0005326, to be published, Europ. Phys. J.
 - ¹² Ch. Niedermeyer, C. Bernhard, T. Blasius, A. Golnik, A. Moodenbaugh, and J.I. Budnick, Phys. Rev. Lett. **80**, 3843 (1998).
 - ¹³ M.-H. Julien, A. Campana, A. Rigamonti, P. Carretta, F. Borsa, P. Kuhns, A.P. Reyes, W.G. Moulton, M. Horvatić, C. Berthier, A. Vietkin, and A. Revcolevschi, cond-mat/0010362.

- ¹⁴ F. Borsa, M. Corti, T. Rega, and A. Rigamonti, Nuovo Cimento **11D**, 1785 (1989).
- ¹⁵ M.-H. Julien, P. Carretta, and F. Borsa, cond-mat/9909351.
- ¹⁶ N.J. Curro, P.C. Hammel, B.J. Suh, M. Hückner, B. Büchner, U. Ammerahl, and A. Revcolevschi, Phys. Rev. Lett. **85**, 642 (2000).
- ¹⁷ F. Cordero, R. Cantelli and M. Ferretti, Phys. Rev. B **61**, 9775 (2000).
- ¹⁸ B.J. Suh, P.C. Hammel, M. Hückner, B. Büchner, U. Ammerahl, and A. Revcolevschi, Phys. Rev. B **61**, 9265 (2000).
- ¹⁹ A.W. Hunt, P.M. Singer, K.R. Thurber, and T. Imai, Phys. Rev. Lett. **82**, 4300 (1999); P.M. Singer, A.W. Hunt, A.F. Cederström, and T. Imai, Phys. Rev. B **60**, 15345 (1999).
- ²⁰ M.C. Chen and C.P. Slichter, Phys. Rev. B **27**, 278 (1983).
- ²¹ A.W. Hunt, P.M. Singer, A.F. Cederstrom, and T. Imai, cond-mat/0011380.